GEOPHYSICAL IMAGING OF ASIA AND SIBERIA: TOMOGRAPHY FOR SEISMIC VELOCITY, UPPER MANTLE GRADIENT, Lg ATTENUATION, AND JOINT INVERSION OF SURFACE WAVE DISPERSION, RECEIVER FUNCTIONS AND SATELLITE GRAVITY DATA

Charlotte A. Rowe[1], William S. Phillips[1], Monica Maceira[1], Michael L. Begnaud, Lee K. Steck[1], Xiaoning (David) Yang[1], Christian L. Lucero[1], Hans E. Hartse[1], Richard J. Stead[1], Kevin G. Mackey[2], Kazuya Fujita[2], and Charles J. Ammon[3]

Los Alamos National Laboratory[1], Michigan State University[2], and Pennsylvania State University[3]

Sponsored by National Nuclear Security Administration
Office of Nonproliferation Research and Development
Office of Defense Nuclear Nonproliferation

Contract No. DE-AC52-06NA25396

ABSTRACT

Our geophysical modeling efforts have focused on a variety of special studies. We continue to develop models for Eastern Russia using the Michigan State Siberia database, for which we have expanded over previous Pn velocity tomography by also inverting Lg amplitudes for a regional attenuation study, and a preliminary tomographic image of Pg travel times in Eurasia, including the Siberia region. Both Lg attenuation and Pg velocity tomographic studies illuminate features consistent with known aspects of Siberian and Russian Far East tectonics and are consistent with features derived in our earlier Pn study. Lg attenuation studies will help to improve our understanding of phase amplitudes for calibration across eastern Russia, and an improved Pg model will allow us to better calibrate travel times in the area when secondary phase arrivals are needed for event location.

We are exploring the effects of upper mantle velocity gradients on the two-dimensional (2-D) tomographic image for P-waves that travel through the upper mantle for regional-distance source-receiver pairs (2.5 to 18 degrees). By adding an upper mantle gradient term to the inversion for 2-D varying Pn velocity and crustal time terms, we are able to map a 2-D varying upper mantle gradient, based on travel times from high-quality event locations. Lateral gradients in the upper mantle across central and eastern Eurasia vary from -0.001 s^{-1} to 0.003 s^{-1}. High gradients appear to be associated with regions of tectonic convergence, both continental and oceanic, as well as stable cratonic regions. Variance reduction is 63% with respect to Pn tomography without gradients. An improved mapping not only of Pn velocities but also of the upper mantle gradients that influence the travel times for this phase is important for ongoing efforts to improve event location throughout central and eastern Asia.

We have recently developed a new joint inversion method using gravity and surface-wave group velocity data, which has been applied to the Tarim and Junggar sedimentary basins in central Asia. The resulting model has been tested and shows a 73% improvement on Rayleigh-wave detection at short periods. Encouraged by these findings, we now present a new three-dimensional (3-D) shear-velocity/density model for the Asian continent constructed through joint inversion of three different geophysical datasets. In addition to the surface wave dispersion values in the period range from 8 to 100 s obtained from the Colorado University Boulder (CUB) Earth model, and gravity observations that were derived from data obtained from the GRACE satellite mission, we also include receiver functions for 45 seismic stations across Asia. Our goal is to investigate the crustal and upper mantle structure beneath the region with increased resolution of shallow geological structures via joint inversion of these three data sets.

Report Documentation Page

Form Approved
OMB No. 0704-0188

1. REPORT DATE	2. REPORT TYPE	3. DATES COVERED
SEP 2007		**00-00-2007 to 00-00-2007**

4. TITLE AND SUBTITLE	5a. CONTRACT NUMBER
Geophysical Imaging of Asia and Siberia: Tomograhy for Seismic Velocity, Upper Mantle Gradient, Lg Attenuation, and Joint Inversion of Surface Wave Dispersion, Receiver Functions and Satellite Gravity Data	5b. GRANT NUMBER
	5c. PROGRAM ELEMENT NUMBER
6. AUTHOR(S)	5d. PROJECT NUMBER
	5e. TASK NUMBER
	5f. WORK UNIT NUMBER
7. PERFORMING ORGANIZATION NAME(S) AND ADDRESS(ES) **Los Alamos National Laboratory,PO Box 1663,Los Alamos,NM,87545**	8. PERFORMING ORGANIZATION REPORT NUMBER
9. SPONSORING/MONITORING AGENCY NAME(S) AND ADDRESS(ES)	10. SPONSOR/MONITOR'S ACRONYM(S)
	11. SPONSOR/MONITOR'S REPORT NUMBER(S)

12. DISTRIBUTION/AVAILABILITY STATEMENT
Approved for public release; distribution unlimited

13. SUPPLEMENTARY NOTES
Proceedings of the 29th Monitoring Research Review: Ground-Based Nuclear Explosion Monitoring Technologies, 25-27 Sep 2007, Denver, CO sponsored by the National Nuclear Security Administration (NNSA) and the Air Force Research Laboratory (AFRL)

14. ABSTRACT
see report

15. SUBJECT TERMS

16. SECURITY CLASSIFICATION OF:			17. LIMITATION OF ABSTRACT	18. NUMBER OF PAGES	19a. NAME OF RESPONSIBLE PERSON
a. REPORT	b. ABSTRACT	c. THIS PAGE			
unclassified	**unclassified**	**unclassified**	**Same as Report (SAR)**	**10**	

OBJECTIVES

To improve calibration capabilities in eastern Eurasia through development of geophysical models and through the acquisition and incorporation of new seismic data for poorly characterized regions.

RESEARCH ACCOMPLISHED

Eastern Russia—Lg Attenuation

We have inverted catalog amplitude parameters to derive a 2D function that maps laterally varying attenuation features for eastern Siberia and the Russian Far East. Data are from the Michigan State University (MSU) Siberia database, compiled through cooperative efforts of MSU, Russian network operators and Los Alamos researchers. In this preliminary analysis we use approximately 280,000 S and Sg amplitude readings from the combined MSU Siberia database. Each independent network (Figure 1) reports corrected amplitude readings for its stations (Mackey et al., 2003). These measurements are in theory frequency-independent, as station response has been removed. We have employed a differential tomographic method, in which each event used must have at least two reporting stations with corrected amplitude readings. Inversion results must be viewed as relative attenuation, rather than absolute.

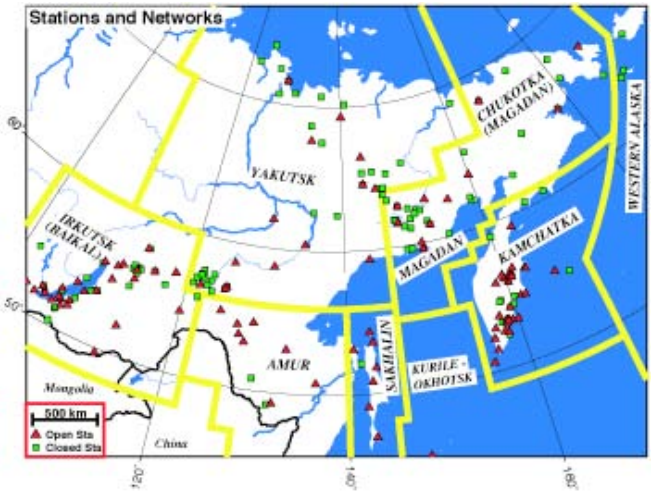

Figure 1. Independent seismic networks contributing to the Siberia database (Mackey et al., 2006).

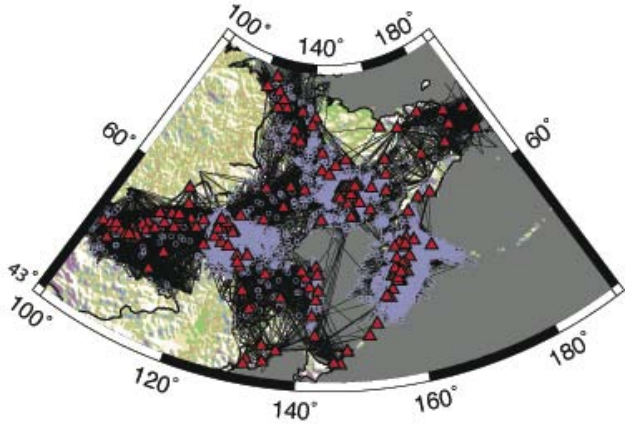

Figure 2. Ray paths used for Lg attenuation tomography.

Figure 2 shows ray paths for data used in the inversion. Events are shown in blue and stations are red triangles. For this preliminary analysis we have not merged the network amplitude data with additional data from our global database, so the coverage is not uniform; for the most part we will be able only to image areas within the individual networks. Tying the Russian network amplitudes in to absolute ground motions will be needed to merge the data sets.

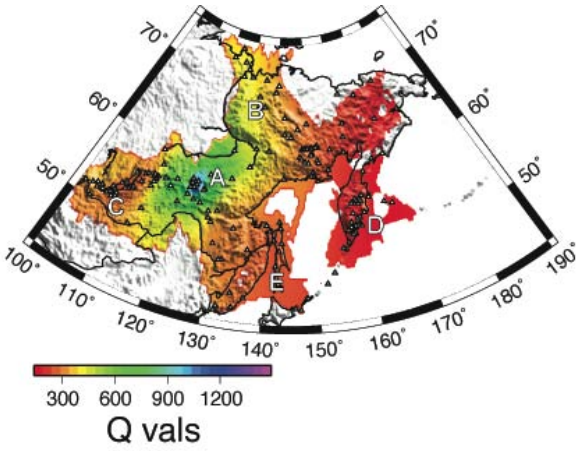

Figure 3. Preliminary Lg Q results.

We performed the tomography using a modification of the Lg-Q tomographic algorithm of Phillips et al. (2000). Since we assume the catalog readings (reported variously as Sg or Lg) were applied to Lg amplitudes, a spreading constant of .83 was used, which is appropriate for surface waves. Signal-to-noise was not constrained due to the lack of reported noise levels, but we assumed that reported amplitudes were adequately large for reliable measurement. The model grid step is ½ degree in both latitude and longitude. We applied a one-sigma data rejection constraint prior to final inversion.

Attenuation variability across northeastern Russia is consistent with expectations for some of the larger tectonic features of the region. Figure 3 shows preliminary results for this analysis. The central high lies within the stable Siberian Platform (A). A rather abrupt drop in Q is observed along the transition to the Verkhoyansk fold belt (B). This is also observed in Pg velocities discussed below. We see a more subtle change in the vicinity of the Baikal Rift (C), where attenuation values are slightly higher to the north and lower to the south. The landward side of the Kamchatka Peninsula (D) exhibits lower Q (higher attenuation) than the seaward side, consistent with differences we would expect between the cold Pacific slab on the east and back-arc materials to the west. Sakhalin Island (E) also exhibits low Q, which corresponds to markedly lower P velocities noted in other studies.

Eastern Russia—Pg Velocity Perturbations

We are undertaking Pg tomography for central and eastern Asia, with a special emphasis on northeastern Russia, to improve travel-time calibration for seismic event locations when secondary phases are used. The data set for this study is comprised of Pg arrivals from 498 seismic stations and over 63,000 events for a total of 266,352 arrivals. We restrict our analysis to crustal earthquakes ($z < 35$ km) and for epicentral distances between 0.6 and 14 degrees. In Figure 4 we show path coverage for this analysis. Data quality control for these arrivals consisted of examining a standard time-distance plot (Figure 5) and excluding any data that falls outside our ad hoc upper and lower bounds (blue and red lines in Figure 5) or if the travel times were negative. Pn contamination in the data is clearly seen in Figure 5, as are timing errors of 30 and 60 s. Larger errors observed are not shown.

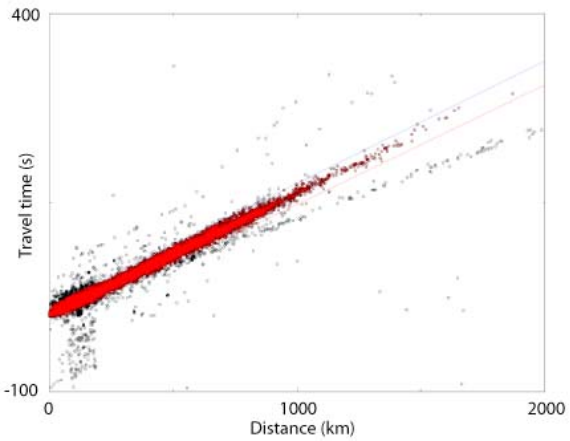

Figure 5. Time-distance plot showing data rejection/inclusion (Steck et al., 2006a).

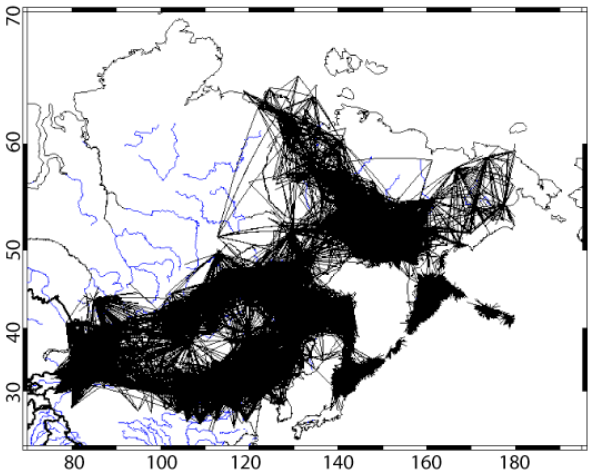

Figure 4. Pg Path coverage (Steck et al., 2006a).

Our method is a first-difference, regularized least-squares inversion, similar to Pn tomography. Travel-time residuals are calculated with respect to the iasp91 Pg travel-time model. The inversion is performed using an LSQR conjugate gradient method, and we solve for slowness perturbations as well as site and event terms. The station term sum is damped to zero while event terms are unconstrained. We assume a great circle path between source and receiver and for this preliminary analysis we do not include event depth, although data selection restricts sources to 35 km or shallower.

In Figure 6 we show the slowness perturbations for the region, with truncation of the color scale for the highest velocity regions: the forearcs of Pacific subduction zones (A and B). Actual slowness perturbations for these two regions exceeded –0.03 s/km. A pronounced velocity low is observed for Sakhalin Island (C), and the Baikal rift shows a velocity low (D), with higher values in the Siberian Platform (E) and Aldan Shield (F).

Site and event terms in this study were relatively small, with minor differences in event terms due largely to the unaccommoded hypocentral depth variations, and large site terms observed primarily in western China and northernmost Japan, where significant crustal thickness and subduction zone complexities, respectively, are likely to cause significant perturbations to average arrival time estimates compared to the iasp91 model.

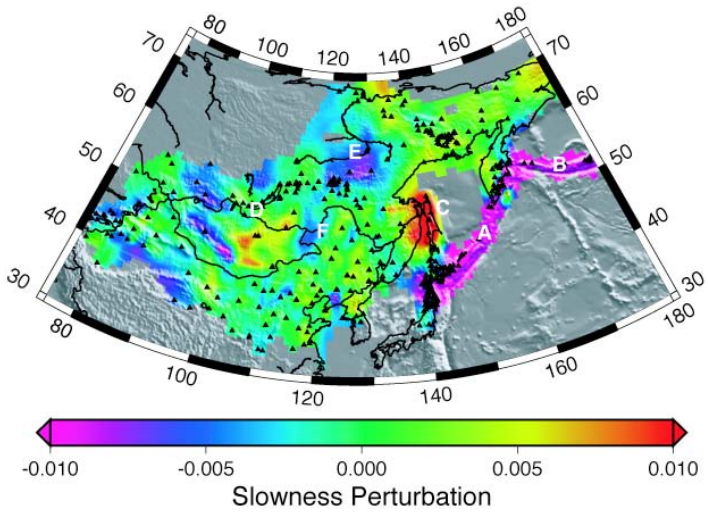

Figure 6. Pg Slowness perturbations (Steck et al., 2006a).

Upper Mantle Pn and Gradient in Eurasia

We explore the effect of laterally varying upper mantle P-wave velocity gradient on our models of Pn perturbations across Eurasia, in an extension of the Zhao (1993) and Zhao and Xie (1993) method. A sharp velocity contrast at the base of the crust and top of the underlying mantle results in a concentration of ray paths for a large variety of source-receiver offsets for crustal earthquakes, which significantly enhances seismologists' ability to image variations in the upper mantle velocity. Regional P-waves are not, however, critically refracted at the crust/mantle interface; rather, due to a combination of upper mantle velocity gradient and earth curvature, they penetrate to varying depths within the mantle, with longer paths sampling deeper regions (e.g., Hearn et al., 2004).

Zhao (1993) and Zhao and Xie (1993) explored the effects of an upper mantle gradient and demonstrated an improved Pn fit through the application of a uniform gradient in some regions. We have extended their method to a 2-D mapping of the gradient (Phillips et al., 2007) and show that these lateral variations in upper mantle gradient are easily obtained along with laterally varying Pn mapping, and the fit to the data is thus improved significantly.

Calculations show that approximate and analytic travel times can be matched with this method to within 1.0 s for a high-gradient mantle ($0.003 s^{-1}$) at 18 degrees offset; moreover, travel times that were ray traced through a laterally varying gradient model similarly matched approximate travel times based on path-averaged gradients. We allow the gradient term to vary in two dimensions by discretizing it in the same manner as for upper mantle velocity, and taking a path average, for inclusion in the tomographic inversion. This gradient term is weakly nonlinear because it requires multiplying gradient and slowness; however, we can address this by setting the average slowness to be constant and adjusting until the regional average slowness is matched. Mantle pierce points are set at 50-degree incidence angles, and model values at each ray segment center are obtained using bilinear interpolation from the surrounding four nodes (e.g., Thurber, 1983). Source and site terms are obtained along with grid-interpolated model parameters for each arrival datum; a linear system of equations is solved via LSQR conjugate gradient (Paige and Saunders, 1982) after applying first-difference constraints.

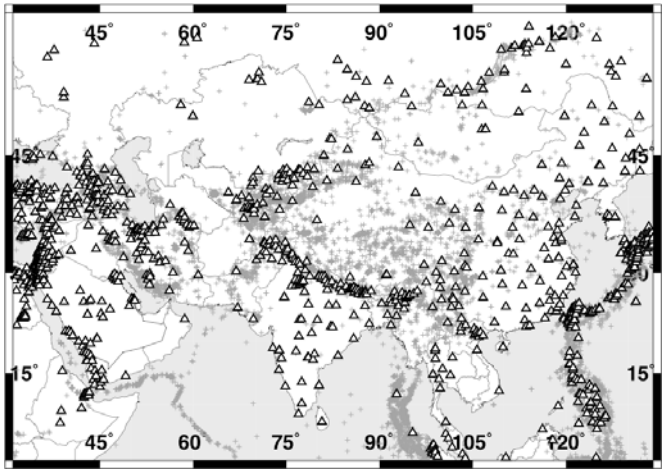

Figure 7.Events and stations contributing travel times for Pn inversion (Phillips et al., 2007).

Data used in this inversion are GT-25 (Bondar et al., 2004) or better. We used 10,396 events and 186,822 arrivals recorded at 1287 stations (Begnaud et al., 2006) within latitude 0–60 degrees north and longitude 30–135 degrees east. Figure 7 shows events (gray dots) and stations (triangles) employed in this study.

We inverted both with and without the gradient, to compare our technique with a standard method, obtaining residual RMS of 2.57 s and 1.57 s for non-gradient and gradient calculations, respectively. Including the gradient provided a variance reduction of 63%, demonstrating significant improvement over non-gradient inversion. These residuals are high compared to some reported in other work: McNamara et al. (1997), Hearn et al.. (2004), Liang et al. (2004), Sun et al. (2004) and Pei et al. (2007) report residual standard deviations of 0.55, 1.3, 1.33, 0.65 and 1.9 s, respectively, while a

differential tomography study (Phillips et al., 2005) reports residuals of 0.96 s. The higher values in our analysis can be attributed to minimal data culling as well as longer distance ranges in this study.

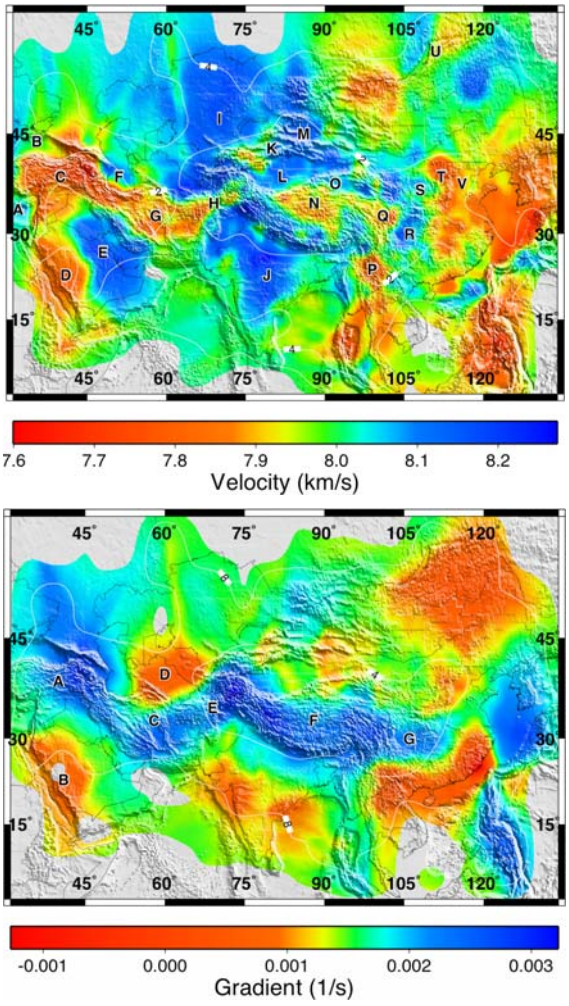

Figure 8. (top) Upper mantle Pn velocities; (bottom) Mantle gradient. Philips et al., 2007).

Our results from the gradient analysis (Figure 8, top) show dramatic differences in magnitude and extent of low velocity anomalies in high gradient areas; for instance, the two adjacent low velocity zones in north-central Tibet (N) and in the Songpan-Ganzi terrane (Q) are much more well-defined than in previous studies. Labels (Figure 8, top) correspond to the following regions: A) East Mediterranean, B) Black Sea, C) Anatolian Plateau, D) Arabian Shield, E) Arabian Platform, F) Caspian Sea, G) Iranian Plateau, H) Hindu Kush, I) Kazakh Shield, J) Indian Shield, K) Tian Shan, L) Tarim Basin, M) Junggar Basin, N) Tibetan Plateau, O) Qaidam Basin, P) Panxi Rift, Q) Songpan-Ganzi, R) Sichuan Basin, S) Ordos Basin, T) Shanxi Graben, U) Baikal Rift, V) North China Basin.

We also see increased definition in the southeastern areas of the low velocity Iranian Plateau (G).

Using longer, thus deeper and faster, paths in these areas degrades our ability to image low-velocity zones when gradients are not accommodated. Note, for instance the sparsely instrumented Tibetan area (N), which requires the use of longer raypaths. Incorporating gradient improves the imaging of low velocity areas that are of tectonic importance.

We observe vertical gradients of upper mantle P velocity from -0.001 to 0.003 s^{-1} in Asia, with an average across Tibet of 0.0025 s^{-1}. The gradient image (Figure 8, bottom) appears to correlate best with known crustal thickness; highs are expected to indicate low thermal gradients in the mantle lid. Labels (Figure 8, bottom) correspond to: A) Anatolian Plateau, B) Arabian shield, C) Iranian Plateau, D) Tajik Basin, D) Hindu Kush, F) Tibetan Plateau, G) Sichuan Basin.

By solving not only for two-dimensional Pn slowness, but also for 2-D upper mantle gradient, we obtain a significant improvement in fit to the data. The inclusion of upper mantle gradient in the inversion allows us in particular to improve the imaging of shallow low-velocity regions, whose slowness estimates are skewed by longer rays sampling deeper paths in an ordinary Pn analysis. The gradients we have obtained appear to be correlated with crustal thickness. The central high in the Tibetan Plateau, of about 0.0025 s^{-1}, is in accordance with the one-dimensional (1-D) gradient found by Zhao and Xie (1993) of 0.003 s^{-1}. Our slightly lower value arises from the damping we have used in the tomographic process, which tends to mute the extrema of a function; we expect somewhat lower values here than in a more focused study.

Joint Tomographic Inversion of Surface Wave Dispersion, Receiver Functions and Satellite Gravity Data

We have recently developed a new joint inversion method using gravity and surface-wave group velocity data, which has been applied to the Tarim and Junggar sedimentary basins in central Asia (Maceira and Ammon, 2007; Steck et al., 2006b). The resulting model has been tested and shows a 73% improvement on Rayleigh-wave detection at short periods (Randall et al., 2006). Encouraged by these findings, we present a new 3-D shear-velocity/density model for the Asian continent constructed through joint inversion of different geophysical datasets. Our goal is to investigate the crustal and upper mantle structure beneath the region with increased

resolution of shallow geological structures via joint inversion of surface-wave group velocities, receiver functions and satellite gravity observations.

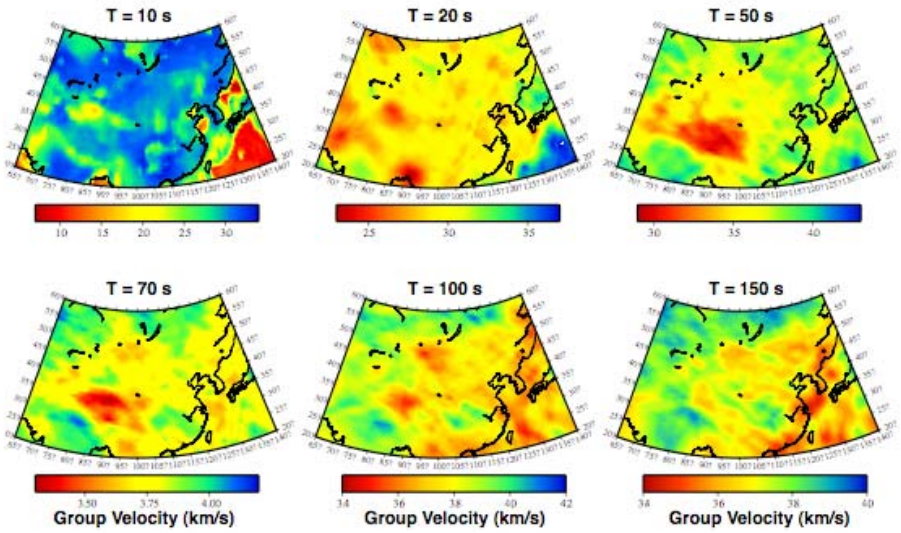

Figure 9. Fundamental mode Rayleigh wave group-velocity maps.

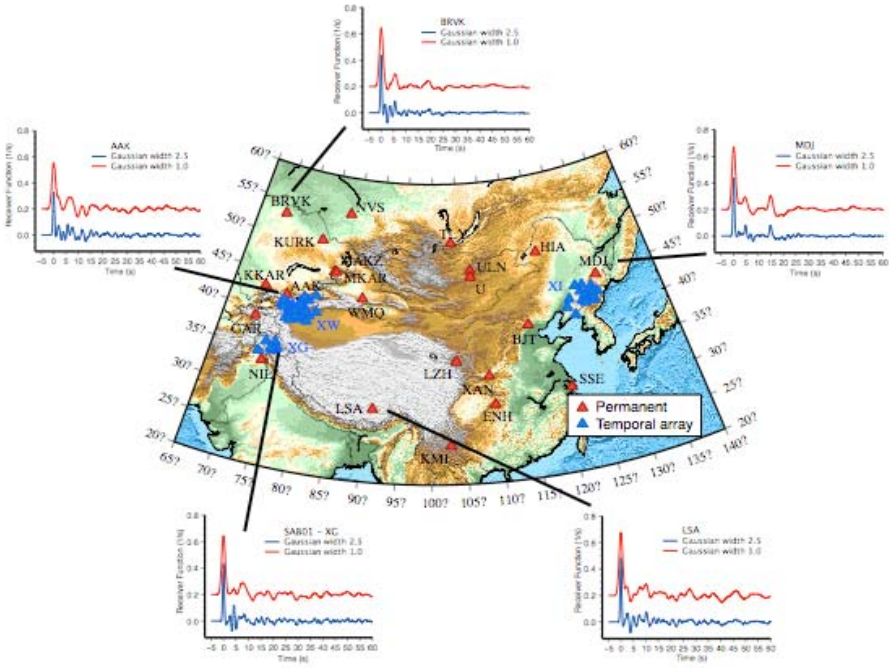

Figure 10. Topographic map of the study region with receiver functions for selected stations.

We parameterize the shear-wave velocity in terms of 1-D depth-dependent velocity profiles determined at the center of each cell in a grid of 1 degree by 1 degree. In each cell we consider three sets of data points: fundamental-mode group velocities, teleseismic P-wave receiver functions and free-air gravity anomalies. Surface wave dispersion measurements are primarily sensitive to vertical shear wave velocity averages, and receiver functions are sensitive to shear wave velocity contrasts and vertical travel-times; hence, shear velocity variations are usually the model parameters in this type of inversion studies. At shallow depths it is difficult to obtain high-resolution dispersion values and constrain the structure because the longer periods are less sensitive to upper crustal structures. Short periods are difficult to measure in tectonically and geologically complex areas. Alternatively, gravity inversions have the greatest resolving power at shallow depths. The gravity measurements supply constraints between seismic velocities and density. Thus by jointly inverting the three data sets, we expect to obtain a self-consistent 3-D shear velocity/density model with increased resolution of shallow geologic structures. Our approach to joint inversion follows the scheme described by Julià et al. (2000), with added gravity anomaly contributions.

Our dispersion velocity data set consists of fundamental mode Rayleigh-wave group velocities. We used the CUB (Colorado University at Boulder) Eurasian tomography model (Ritzwoller and Levshin, 1998; Levshin et al., 2001, 2002) in the period range between 8 and 150 s.

In general, the tomographic patterns in the CUB model show a very good correlation with known geologic and tectonic features in the area. Figure 9 shows fundamental mode Rayleigh wave group-velocity maps extracted from the CUB model that are used in the preliminary, simultaneous inversions of dispersion, receiver function and gravity, outlined below. Note that the color scale varies to preserve the details in each image.

We used teleseismic P-wave receiver functions (Ammon et al., 2004) for 45 stations across eastern Asia. Figure 10 shows a topographic map of the region under study; triangles represent stations analyzed in the receiver function analysis of Ammon et al. (2004). Sample receiver functions (in 2 bandwidths) are shown for selected stations. Initial peak on the receiver functions is generated by incident P arrival; subsequent arrivals are P-S converted waves from the structure beneath the recording station.

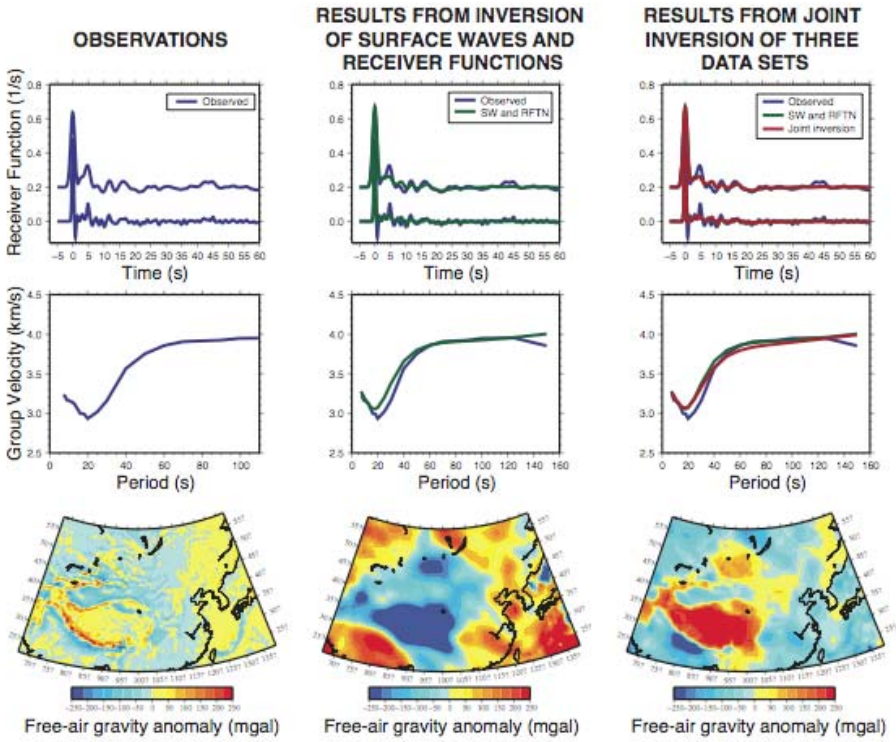

Figure 11. Observations, fit using surface wave dispersion and receiver functions, and fit using these plus satellite gravity.

Gravity observations were obtained from the Gravity Recovery and Climate Experiment (GRACE) satellite mission (Tapley et al., 2005).

An iterative, conjugate gradient-based least squares inversion is used to jointly model the three different data sets, using shear-velocity variations as the primary model parameters.

Figure 11 provides a comparison of the results of inversions of surface-wave dispersion observations and receiver functions, and gravity, surface wave dispersion and receiver functions. Top panels from left to right: receiver function (RFTN) data for a specific cell in our model (blue line); fit to the RFTN data from jointly inverting surface wave dispersion (SWD) and RFTN (green line); fit to the RFTN data from the joint inversion of the three data sets (red line). Middle panels from left to right: SWD data for the same typical cell (blue line); fit to the SWD from only inverting SWD and RFTN data (green line); fit to the SWD from the joint inversion of the three data sets (red line). Bottom panels from left to right: GRACE data for the region under study; predicted free-air gravity anomalies from the model resulting from inverting SWD and RFTN observations; predicted free-air gravity anomalies from the model resulting from the joint inversion of SWD, RFTN, and gravity observations.

The underlying philosophy of this effort is that the combination of the three types of data produces a more consistent Earth model. These results are preliminary and are primarily shown to illustrate the basic concepts in the analysis. Additional work is needed to improve and correctly predict the free-air gravity over such a large region.

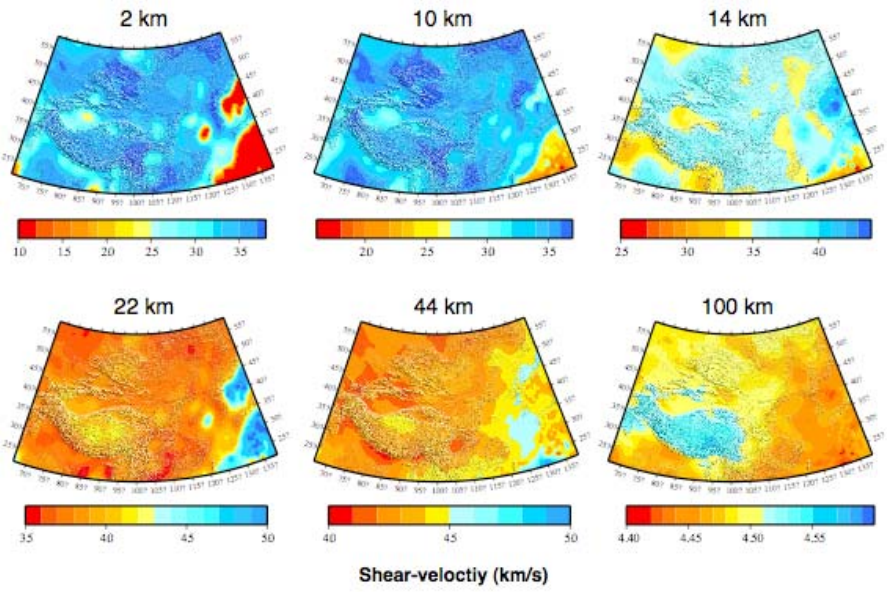

Figure 12. Preliminary shear velocity model for study area, determined through joint inversion of the three data sets.

Figure 12 shows the preliminary shear velocity model for Asia based on joint inversion of receiver function, dispersion curves and gravity; depth slices from six levels in the model are shown. Over a smaller region, Maceira and Ammon (2007) show that the addition of gravity observations can help sharpen structures blurred in surface-wave tomography. Here, high wave number signals in the deep parts of the model (where none of the data have the sensitivity or coverage to constrain such structures) suggest the mapping of shallow structure artifacts into the deeper parts of the shear-velocity model. More work is needed and planned on the integration of gravity and seismic signals over this large region.

CONCLUSIONS AND RECOMMENDATIONS

Results presented here confirm that innovative directions of research and important new data are improving the accuracy and applicability of our geophysical models for eastern Eurasia. The tremendous volume of new data at our disposal via the Siberian catalog is allowing us to undertake detailed modeling of this region that previously was poorly characterized in terms of its geophysical parameters. As new ways of addressing the complexities within the Earth are devised, we are able to incorporate a better understanding of their influence on our data products—such as the upper mantle gradient innovation in 2-D Pn mapping. Incorporating multi-parameter data sets, such as the satellite gravity in combination with seismic parameters, helps us to constrain inversions that previously were subject to ambiguity when only one type of data is used.

REFERENCES

Ammon, C. J., W. Sevilla, R. B. Herrmann, and G. E. Randall (2004). Systematic inversion of receiver functions and surface wave dispersion for crustal structure in central Asia, in *Proceedings of the 26th Seismic Research Review: Trends in Nuclear Explosion Monitoring*, LA-UR-04-5801, Vol.1, pp. 29–38.

Begnaud, M .L., L. K. Steck, and C. A. Rowe (2006). Improving seismic event locations in Asia by using catalog-scale empirical travel time correction surfaces, *EOS, Trans. AGU* 87: Fall Meet. Suppl. Abstract T51D-1550.

Bondar, L .S., C. Myers, F. R. Engdahl, and F.A. Bergman (2004), Epicentre accuracy based on seismic network criteria, *Geophys. J. Int.* 156: 483–496.

Hearn, T. M., S. Wang, J. F. Ni, Z. Xu, Y. Yu, and X. Zhang (2004). Uppermost mantle velocities beneath China and surrounding regions, *J. Geophys. Res.* 109: B11301, doi:10.1029/2003JB002847.

Julià, J., C. J. Ammon, R. B. Herrmann, and A. M. Correig (2000). Joint inversion of receiver function and surface wave dispersion observations, *Geophys. J. Int.* 143: 99–112.

Levshin, A. L., M. H. Ritzwoller, M. P. Barmin, and J. L. Stevens (2001). Short period group velocity measurements and maps in central Asia, in *Proceedings of the 23rd Seismic Research Review: Worldwide Monitoring of Nuclear Explosions*, LA-UR-01-4454, Vol. 1, pp. 258–269.

Levshin, A. L., J. L. Stevens, M. H. Ritzwoller, and D. A. Adams (2002). Short-period (7-s to 15-s) group velocity measurements and maps in central Asia, in *Proceedings of the 24th Seismic Research Review—Nuclear Explosion Monitoring: Innovation and Integration*, LA-UR-02-5048, Vol. 1, pp. 97–106.

Liang, C., X. Song, and J. Huang (2004). Tomographic inversion of Pn travel times in China, *J. Geophys. Res.* 109: B11301, doi:10.1029/2003JB002789.

Maceira, M. and C. J. Ammon (2007). Joint inversion of surface wave velocity and gravity observations and its application to Central Asian basins shear velocity structure, *J. Geophys. Res.* (submitted).

Mackey, K. G., K. Fujita, L. K. Steck, and H. E. Hartse (2003). Seismic regionalization in eastern Russia, in *Proceedings of the 25th Seismic Research Review—Nuclear Explosion Monitoring: Building the Knowledge Base*, LA-UR-03-6029, Vol. 1, pp. 73–82.

Mackey, K., H. E. Hartse, K. Fujita, L. Linkimer, L. Steck, R. Stead, and C. Rowe (2006). Seismic characterization of northeast Asia, in *Proceedings of the 28th Seismic Research Review: Ground-Based Nuclear Explosion Monitoring Technologies*, LA-UR-06-5471, Vol. 1, pp. 93–102.

McNamara, D. E., W. R. Walter, T. J. Owens, and C. J. Ammon (1997). Upper mantle velocity structure beneath the Tibetan Plateau from Pn travel time tomography, *J. Geophys. Res*. 102: 493–505.

Paige, C. C. and M. A. Saunders (1982). Algorithm 583, LSQR: Sparse linear equations and least-squares problems, *ACM Trans. Math Software* 8: 195–209.

Pei, S., J. Zhao, Y. Sun, Z. Xu, S. Wang, H. Liu, C. A. Rowe, M. N. Toksoz, and X. Gao (2007). Upper mantle seismic velocities and anisotropy in China determined through Pn and Sn tomography, *J. Geophys. Res*. 122: B05312, doi:10.1029/2006JB004409.

Phillips, W. S., H. E. Hartse, S. T. Taylor, and G. R. Randall (2000). 1 Hz Lg tomography in central Asia, *Geophys. Res. Lett*. 22: 3425–428.

Phillips, W. S., C. A. Rowe, and L. K. Steck (2005). The use of interstation arrival time differences to account for regional path variability, *Geophys. Res. Lett*. 32: L11301, doi:10.1029/2005GL022558.

Phillips, W. S., M. L. Begnaud, C. A. Rowe, L .K. Steck, S. C. Meyers, M. E. Pasyanos and S. Ballard (2007). Accounting for lateral variations of the upper mantle gradient in Pn tomography studies, *Geophys. Res. Lett*. (in press).

Ritzwoller, M. H. and A. L. Levshin (1998), Eurasian surface wave tomography: group velocities, *J. Geophys. Res*. 103: 4839–4878.

Steck, L. K., M. L. Begnaud, C. A. Rowe, and H. E. Hartse (2006a). Improved seismic event locations in Siberia using empirical and model-based travel-time corrections. *EOS, Trans, AGU*. 87: Fall Meeting Suppl., Abstract T51D-1549.

Sun, Y., X. Li, S. Kueli, F.D. Morgan, and M. N. Toksoz (2004). Adaptive moving window method for 3D P-velocity tomography and its application in China, *Bull. Seismol. Soc. Am*. 94: 740–746.

Thurber, C. H. (1983). Earthquake location and three-dimensioal crustal structure in the Coyote Lake area, central California, *J. Geophys. Res*. 88: 8226–8236.

Zhao, L.-S. (1993). Lateral variations and azimuthal isotropy of Pn velocities beneath Basin and Range Province, *J. Geophys. Res*. 98: 22109–22122.

Zhao, L-S. and J. Xie (1993). Lateral variations in compressional velocities beneath the Tibetan Plateau from Pn travel time tomography, *Geophys. J. Int.* 115: 1070–1084.